Airborne and spaceborne DEM- and laser altimetry-derived surface elevation and volume changes of the Bering Glacier system, Alaska, USA, and Yukon, Canada, 1972–2006

Reginald R. MUSKETT,[1] Craig S. LINGLE,[1] Jeanne M. SAUBER,[2] Austin S. POST,[3] Wendell V. TANGBORN,[4] Bernhard T. RABUS,[5] Keith A. ECHELMEYER[1]

[1]*Geophysical Institute, University of Alaska, 903 Koyukuk Drive, Fairbanks, Alaska 99775-7320, USA*
E-mail: rmuskett@iarc.uaf.edu
[2]*NASA Goddard Space Flight Center, Code 698, Greenbelt, Maryland 20902, USA*
[3]*2014 Bradley Street, Dupont, Washington 98327, USA*
[4]*HyMet, Inc., 13639 Burma Road SW, Vashon, Washington 98070, USA*
[5]*MacDonald Dettwiler, 13800 Commerce Parkway, Richmond, British Columbia V6V 2J3, Canada*

ABSTRACT. Using airborne and spaceborne high-resolution digital elevation models and laser altimetry, we present estimates of interannual and multi-decadal surface elevation changes on the Bering Glacier system, Alaska, USA, and Yukon, Canada, from 1972 to 2006. We find: (1) the rate of lowering during 1972–95 was $0.9 \pm 0.1\,m\,a^{-1}$; (2) this rate accelerated to $3.0 \pm 0.7\,m\,a^{-1}$ during 1995–2000; and (3) during 2000–03 the lowering rate was $1.5 \pm 0.4\,m\,a^{-1}$. From 1972 to 2003, 70% of the area of the system experienced a volume loss of $191 \pm 17\,km^3$, which was an area-average surface elevation lowering of $1.7 \pm 0.2\,m\,a^{-1}$. From November 2004 to November 2006, surface elevations across Bering Glacier, from McIntosh Peak on the south to Waxell Ridge on the north, rose as much as 53 m. Up-glacier on Bagley Ice Valley about 10 km east of Juniper Island nunatak, surface elevations lowered as much as 28 m from October 2003 to October 2006. NASA Terra/MODIS observations from May to September 2006 indicated muddy outburst floods from the Bering terminus into Vitus Lake. This suggests basal–englacial hydrologic storage changes were a contributing factor in the surface elevation changes in the fall of 2006.

INTRODUCTION

Bering Glacier (Fig. 1), the main glacier of the system of connected glaciers and icefields in south-central Alaska, USA, and southwestern Yukon, Canada, is the largest surging piedmont glacier (Molnia, 2001). Bering Glacier (including Bagley Ice Valley) last surged in 1993–95 (Fatland 1998; Fatland and Lingle, 2002; Lingle and Fatland, 2003; Roush and others, 2003). A minor surge was observed in 1981 (Molnia and Post, 1995). Other major surges were observed in 1965–66 and 1957–60 (Post, 1972). Glaciers forming the system have varied flow characteristics. Jefferies and Tana Glaciers have not been observed surging. Steller Glacier exhibits brief periods of fast flow which are less than that of surging flow (Post, 1972). This leads to complications in describing the system and estimating mass balance (Beedle and others, 2008). Equilibrium lines, estimated from late-summer firn lines seen in air photography dating from the 1950s to the 1970s, have ranged from about 900 to 1100 m elevation (Molnia and Post, 1995). The region including the Bering Glacier and Malaspina Glacier systems, Hubbard Glacier and the glaciers of the Wrangell Mountains is the largest glacierized region in continental North America (Molnia, 2001).

Basal water has been identified as a key component in basal sliding, such as in transient speed-ups associated with heavy precipitation and supraglacial lake floods (Fountain and Walder, 1998; Kavanaugh and Clarke, 2000; Bartholomaus and others, 2008). The glacier basal hydrologic system has been identified as a trigger in glacier surging once the glacier system has obtained a pre-surge thickness (Raymond, 1987; Fountain and Walder, 1998; Harrison and Post, 2003; Lingle and Fatland, 2003).

We present an investigation of the surface elevation changes of the Bering Glacier system through analysis of airborne- and spaceborne-derived digital elevation datasets. The investigation period is late summer 1972 to fall 2006. Here we report on recent observations of outburst flood events of summer 2006 and associated surface elevation changes, and the multi-decadal area-average surface-elevation changes during 1972–2003.

DATA AND METHODS

Our analysis of surface elevation changes of the Bering Glacier system derives from a combination of moderate- and high-resolution spaceborne imagery from the NASA Terra satellite, and surface elevation datasets derived from airborne and spaceborne systems (Table 1; Fig. 2). We begin by listing these in order below; more details are given in Table 1.

Spaceborne imagery

1. NASA Terra Advanced Spaceborne Thermal Emission and Reflection Radiometer (ASTER; Yamaguchi and others, 1998; Abrams and Hook, 2002) imagery acquired August 2003 to 2006.

2. NASA Terra moderate-resolution imaging spectroradiometer (MODIS) imagery acquired in summer and fall of 2002–06 (Toller and Isaacman, 2003).

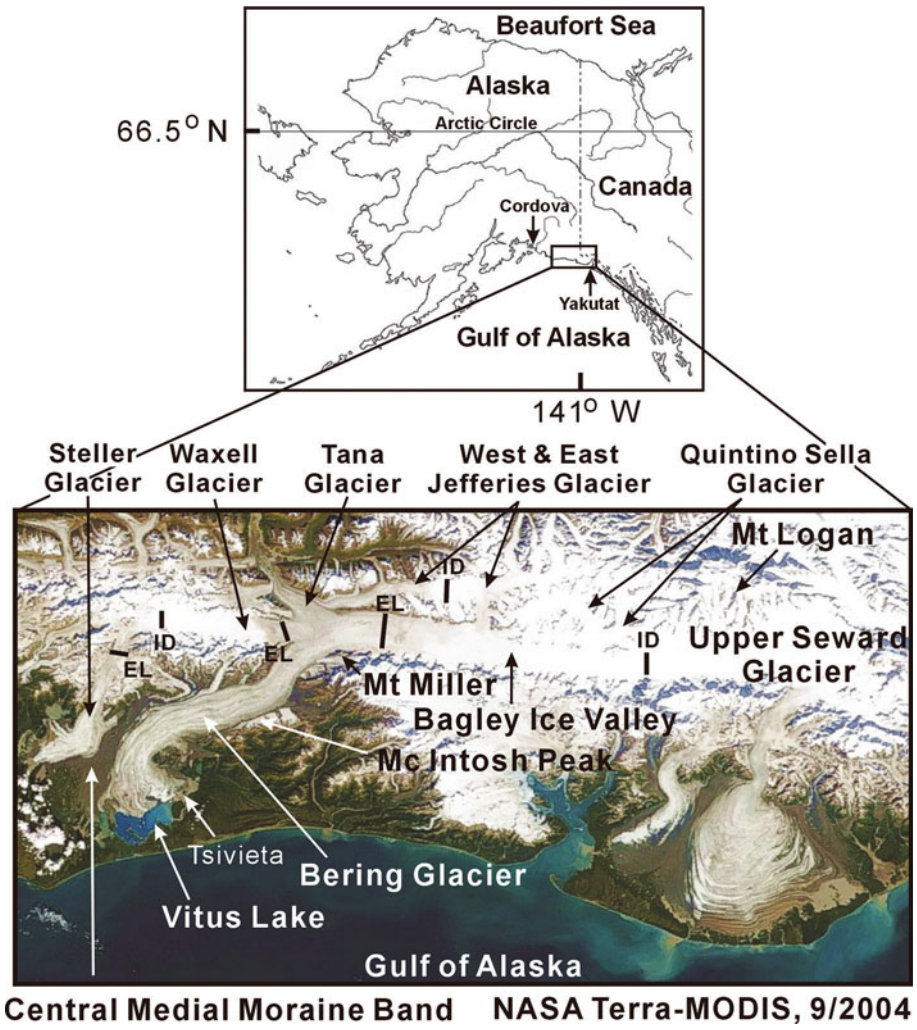

Fig. 1. Bering Glacier system, eastern Chugach and St Elias Mountains, south-central Alaska, as seen on 9 September 2004 (NASA Terra/MODIS). The part of Bagley Ice Valley adjacent to Upper Seward Glacier, Yukon, is named Columbus Glacier by the US Board on Geographic Names. ID marks the locations of ice divides. EL marks the locations of long-term equilibrium lines.

3. European Remote-sensing Satellite (ERS-1/-2) tandem mission synthetic aperture radar (SAR) amplitude backscatter data acquired in winter 1995 (Rignot and Van Zyl, 1993).

Airborne and spaceborne digital elevation datasets

1. Airborne-derived interferometric synthetic aperture radar (InSAR) digital elevation models (DEMs), produced by Intermap Technologies, Inc., acquired during 4–13 September 2000 and 3–4 August 2002 (Intermap, 2006).
2. Airborne-derived surface elevation data acquired by small aircraft 5 June 1995, 23 June 2000, 26 August 2000 and 22 August 2003 (Echelmeyer and others, 1996).
3. NASA Shuttle Radar Topography Mission (SRTM) DEMs produced at the Deutsches Zentrum für Luft- und Raumfahrt (DLR, X-band, special acquisitions) and the NASA Jet Propulsion Laboratory (JPL, C-band), acquired 11–22 February 2000 (Geudtner and others, 2002; Helm and others, 2002; Rabus and others, 2003; Farr and others, 2007).
4. NASA Terra/ASTER DEM generated from imagery acquired 3 August 2003. It was adjusted using airborne laser altimetry acquired August 2003 for vertical bias control.

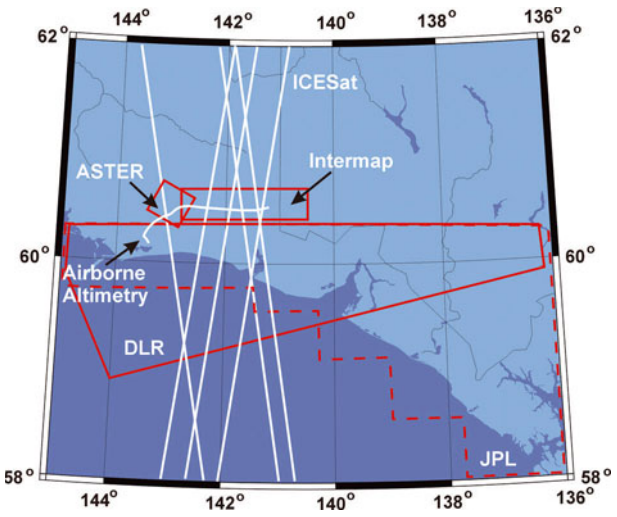

Fig. 2. Area coverage of the digital elevation datasets and lines representing the airborne and spaceborne altimetry.

Table 1. Elevation data sources

Source	Datum	Spatial posting	Spectral channel	Vertical rmse*	Acquisition year
Spaceborne altimeter:					
ICESat	TOPEX/Poseidon	70 x 172 m, 10 km	1064 nm	0.15–0.30 m	2003–06
Spaceborne interferometric synthetic aperture radar:					
SRTM, X-band, DLR	WGS84 EGM96/	25 x 25 m	9.6 GHz, VV	6 m, 16 m	2000
C-band, JPL	WGS84	30 x 30 m	5.3 GHz, Dual	6 m, 16 m	
Airborne interferometric synthetic aperture radar:					
Intermap Technologies, Inc.	EGM96/WGS84	10 x 10 m	9.6 GHz, HH	2.5 m	2000
Airborne altimeter:					
Small-aircraft laser altimeter	GEOID99/WGS84	0.2 x 1.2 m	905 nm	0.30 m	1995/2000/2003
Airborne photographic/cartographic:					
Center for Topographic Information, Natural Resources Canada	NGVD29/NAD27	2 x 3 arcsec	Panchromatic	1/2 contour	1976
USGS	NGVD29/NAD27	2 x 3 arcsec	Panchromatic	1/2 contour	1971/72

*Root-mean square error.

5. Spaceborne-derived surface elevation data from the Ice, Cloud and land Elevation Satellite (ICESat) acquired during October–November 2003, 2004 and 2006 (Schutz and others, 2005).
6. United States Geological Survey (USGS) and Natural Resources Canada Center for Topographic Information DEMs, the elevations of which originate from maps produced from aerial photography in the late summer of 1972, 1973 (US) and 1976 (Canada) (USGS, 1990; Natural Resources Canada, 1996).

The Intermap Technologies, Inc. airborne surveys covered 5000 km^2 of the Bering and Malaspina Glacier systems, 10 000 km^2 in total (Muskett, 2007). The NASA/DLR DEM we use covers a region of 51 000 km^2 in south-central Alaska and Yukon, approximately 59–60.3° N, 136–144° W (Eineder and others, 2001; Roth and others, 2001; Rabus and others, 2003). NASA JPL DEMs (version 1, C-band) cover land area up to 60.3° N; final versions to 60° N (Farr and others, 2007).

ICESat altimeter tracks crossing the Bering Glacier system derive from ascending–descending orbits (Schutz and others, 2005). At 60° N, cross-track spacing was variable, as close as 10 km along Bagley Ice Valley (Fig. 2). ICESat footprints cover a surface area of 50–70 m diameter spaced about 172 m along-track. For track-to-track differencing we selected exact- (overlapping footprints) and near-repeat tracks (about 60 m transverse separation). The close positions of the footprints on very low-slope glacier surfaces eliminate a slope adjustment, which could be the case for large cross-track separations of 10 km or more (Scambos and others, 2004). Selection of ICESat tracks for surface elevation change was made based on consideration of Laser 2 and 3 campaigns performance, and thin-cloud to cloud-free conditions (elevation channel waveforms and cloud channel backscatter data), and with comparison to near-co-temporal NASA Terra/MODIS imagery.

Datum, grid and reference frame

The datasets were transformed to a common datum, the World Geodetic System 1984 (WGS84), which includes a worldwide network of global positioning system (GPS) receiver stations, i.e. reference frame (the International Terrestrial Reference Frame), a best-fitting ellipsoid model (the WGS84 ellipsoid) and a geoid model (the Earth Gravity Model 1996 (EGM96)) (NIMA, 2000). WGS is referred to as a non-tide geodetic system (Rapp, 1998). We used a degree-order 360 by 360 spherical harmonic coefficients file and programs provided by the US National Geospatial-Intelligence Agency, which are freely available online, to remove the EGM96 geoid heights from the high-resolution Intermap and SRTM (JPL) DEMs (http://earth-info.nga.mil/GandG/). We used high-resolution geoid data from the US National Oceanic and Atmospheric Administration (NOAA) National Geodetic Survey, GEOID99-Alaska; it is a 1 arc min model derived from additional gravity measurements and EGM96 (Smith and Roman, 2001) (Fig. 3a).

The DEM datasets were bilinearly resampled to 30 m × 30 m grids (pixel sizing) and projected into the Universal Transverse Mercator system (an equal-area projection system) (Muskett, 2007). Co-registration of the datasets was achieved by using feature locations derived from the Intermap DEM, matched to the same features in the SRTM, USGS and Canada DEMs. This derived *x-y* plane offsets, which were then minimized using a first-order polynomial surface through the least-squares technique. The horizontal control datum of the USGS and Canada DEMs, the North American Datum 1927 (NAD27), which adopts the Clarke 1866 ellipsoid, was transformed to the WGS84 ellipsoid (this had no effect on the vertical control datum, the National Geodetic Vertical Datum 1929 (NGVD29)).

The ICESat surface elevations come from the global elevation datasets GLA06, provided by the US National Snow and Ice Data Center. ICESat surface elevation data are relative to the TOPEX/Poseidon ellipsoid (a member of the mean-tide reference ellipsoids and reference frames). We use a program provided by JPL (courtesy of R. Guritz, Alaska Satellite Facility), augmented by us to transform the ICESat elevations to reference the WGS84 ellipsoid. By design, the TOPEX/Poseidon equatorial and polar radii are 0.70 and 0.71 m shorter, respectively, than those of WGS84.

NASA ASTER imagery (band 3N (nominal nadir-pointing) and 3B (nominal back-pointing)) acquired on 3 August 2003 was used for DEM generation. The stereo pair was processed using the Environment for Visualization (ENVI)–Interactive Data Language (IDL) software. The generated DEM covers parts of Bering, Tana and Waxell Glaciers and lower Bagley Ice Valley. The ASTER DEM was bilinearly up-sampled to a 30 m × 30 m grid. The oblique stereo geometry in tight-spaced high-relief mountainous regions can offer some difficulty to DEM generation (Matthews and others, 2008; Toutin, 2008). On relatively flat terrain, ASTER-derived DEMs have nominal accuracy similar to USGS DEMs (Kieffer and others, 2008). In all cases, the latest-date DEMs and altimetry were assumed to be the most accurate and functioned as the reference surface of the glaciers for deriving surface elevation changes.

Snow accumulation adjustments

The Intermap and SRTM DEMs and ICESat-derived elevations were adjusted for estimated winter snow accumulation from 1 September to the day of data acquisition (Muskett and others, 2003, 2008a,b; Muskett, 2007). When differencing ICESat-to-ICASat same-month different-year elevations, snow accumulation adjustments were not applied. The adjustment for SRTM and ICESat used published surface snow densities, which range from about 550 kg m^{-3} at about 450 m elevation to 350 kg m^{-3} at 2400 m elevation (Sharp, 1951, 1958; Alford, 1967). An estimate of winter surface snow density was based on Zwally and Li (2002). The adjustment for the Intermap DEM relied on an estimated surface snow density (fresh snow) of 200 kg m^{-3}. Daily meteorological observations of precipitation and temperature come from the US National Weather Service stations at Cordova and Yakutat. Area–elevation distributions of the Bering and Malaspina Glacier systems from the early-date DEMs provided for elevation references. These were incorporated into the precipitation–temperature–area altitude glacier mass-balance model of Tangborn (1999) to estimate snow accumulation throughout the elevation distributions in water equivalent. Surface density curves provided for conversion of the snow water equivalents into snow equivalents. Zhang and others (2007) found the Tangborn model compared well with USGS mass balance estimated on Gulkana Glacier. Figure 3b shows the estimated snow accumulation (i.e. snow depths as a function of elevation) used to adjust the Intermap DEM.

Adjustments for systematic vertical errors

We estimated vertical bias between the elevations of the co-registered datasets on non-glacierized terrain (Muskett and others, 2003, 2008a,b; Muskett, 2007). Another variety of vertical offset, from an exaggeration of contour shape, was estimated by comparison of Intermap and USGS/Canada DEM contours. The estimates of vertical biases were then used as adjustments to the area-averaged surface elevation changes.

The vertical accuracy of the Intermap DEM was verified with a comparison with an airborne laser altimeter profile acquired on 26 August 2000, along the center flowline of Bagley Ice Valley between 1100 and 1875 m elevation (Fig. 3c). The comparison on a same-datum WGS84 ellipsoid basis with snow accumulation adjustment had a difference (mean and standard deviation) of –1.3 ± 0.9 m (Intermap DEM lower). This difference is probably an

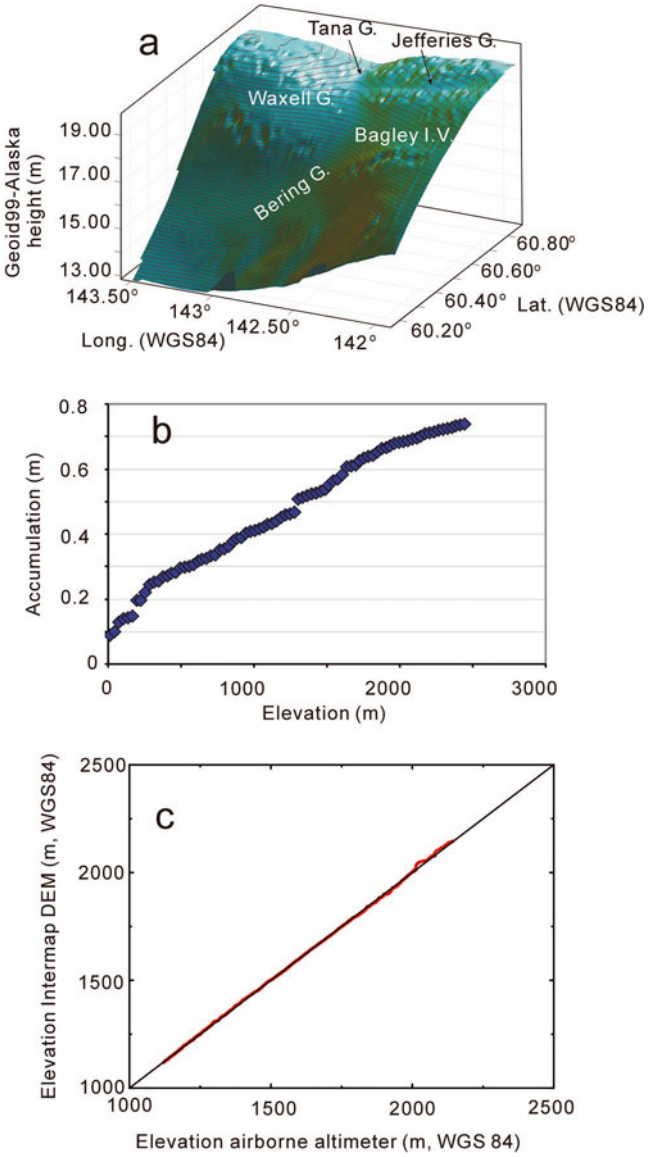

Fig. 3. (a) GEOID99-Alaska geoid heights in the area of the ASTER DEM. Note the troughs in the geoid heights on Bering Glacier, Bagley Ice Valley/Waxell Glacier and Tana Glacier in particular. The long axis of the geoid height undulation is north of Jefferies Glacier. (b) Estimated snow accumulation (i.e. snow depth) from 26 August to 13 September, as a function of elevation (relative to mean sea level) used to adjust the Intermap DEM. (c) Intermap DEM compared with airborne altimeter elevations on same-location and -datum basis.

expression of the X-band penetration depth. Variation of the X-band penetration depth along the profile was likely due to changes in water content (Partington, 1998).

Penetration depth of the SRTM C-band radar relative to the X-band radar on glacier ice was estimated on the Bering Lobe (Muskett, 2007). We estimated the C-band radar penetration below the X-band penetration depth was 1.1 ± 3.6 m. This is in the range of estimated C-band penetration depths reported by Rignot and others (2001) at similar surface elevations on Brady Glacier, Alaska. Radar penetration depths are dependent on radar frequency (less for high frequency X- and C-bands, and greater for low frequencies in the L-band) and are highly sensitive to grain-boundary water content (Li and others, 1999). Grain-boundary water content as low as 2% can reduce radar

penetration depth by an order of magnitude relative to the dry grain-boundary condition (Partington, 1998). Over the period 1972–2006 we assumed an approximation of Sorge's law, i.e. the rate of densification of firn was invariant in time over this period (Bader, 1954).

Glacier area extractions

ERS-1/2 tandem mission datasets covering the Bering, Malaspina and Icy Bay Glacier systems were processed, terrain-corrected, and co-registered with the USGS/Canada DEM mosaic (Muskett and others, 2003, 2008a,b; Muskett, 2007) (Fig. 4). The radar backscatter images and co-registered digital slope models were used to build glacier area masks for the extraction of elevation data on the glaciers of the Bering Glacier system. Radar backscatter is highly sensitive to grain-boundary water content and surface emissivity (Rignot and Van Zyl, 1993; Partington, 1998). Only on the highest elevations of Mount Logan are there indications of a dry-snow or percolation facies (Li, 1999). The glacier surfaces we investigate are well below the elevations of the summit of Mount Logan. Coastal Alaska and Yukon have enjoyed increased precipitation (rainfall) year-round, and particularly in January, since about 1976/77 (Moore and others, 2002; Muskett and others, 2003, 2008a,b).

Area-average surface elevation changes

We employ the formalism of Meier (1962) in the fixed-date system (Anonymous, 1969) to estimate glacier net mass balance, $\dot{\overline{b}}$, i.e. the area-average surface elevation change,

$$\dot{\overline{b}} = \Delta V / \overline{A} / \Delta t \quad (1)$$

where ΔV is the integrated volume change through the mean glacier area during Δt, $\overline{A}$ is the mean glacier area during Δt, and Δt is the time interval, preferably (or approximately) an integer number of years. This formalism allows us to estimate the area-average surface elevation changes within parts of the Bering Glacier system, i.e. the surging glaciers relative to the non-surging glaciers, as well as those changes on ablation regions (water equivalent) relative to accumulation regions (ice equivalent), and the integrated total area covered by the most recent DEMs.

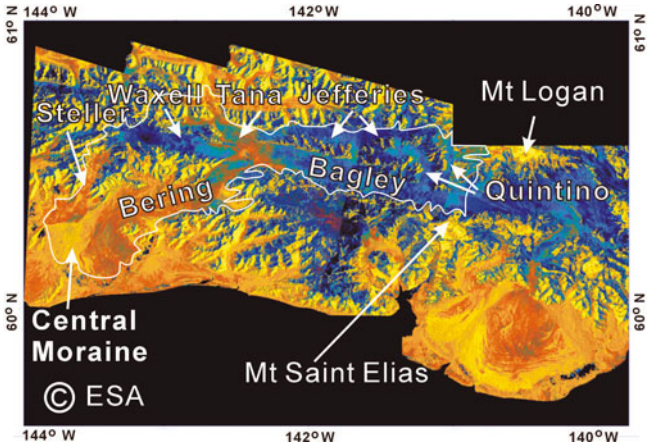

Fig. 4. European Space Agency tandem mission synthetic aperture radar terrain-corrected mosaic of the Bering Glacier system and other glaciers in south-central Alaska. Mount Logan, Mount Saint Elias and the glaciers of interest are located. A generalized system boundary is shown. The colorization of the σ^0 backscatter digital numbers aids in distinguishing radar snow facies.

RESULTS

DEM multi-decadal surface-elevation changes

Figure 5 shows the difference DEMs covering the Bering Glacier system. Area-averaged surface elevations and volume changes are given in Table 2. Surface-elevation changes are spatially non-uniform. The largest magnitudes of surface-elevation lowering occur on parts of the glacier

Table 2. Area-average surface elevation changes

Glacier	A	ΔV	ΔE	Extremes	$\Delta V/A$	Δt	$\Delta V/\overline{A}/\Delta t$
	km^2	km^3	m	m	m		m a^{-1}
Intermap DEM (2000) minus USGS (1972/73) or Canada DEM (1976)							
(1) Bagley Ice Valley	168	−5 ± 2	−50 ± 9		−28 ± 9	1972–2000	−1.0 ± 0.3
(2) Bagley Ice Valley	575	+7 ± 3	−40 ± 6	+100 ± 6	+13 ± 6	1972–2000	+0.5 ± 0.2
(3) Columbus Glacier	187	+6 ± 1	−30 ± 6	+120 ± 6	+34 ± 6	1972–2000	+1.2 ± 0.2
(4) Ice divide area	157	−2 ± 1	−90 ± 4	+160 ± 4	−10 ± 6	1976–2000	−0.4 ± 0.2
(5), Quintino Sella Glacier	257	−12 ± 1	−250 ± 5	+50 ± 5	−47 ± 5	1976–2000	−1.9 ± 0.2
(6), E. Jefferies Glacier	242	−3 ± 2	−50 ± 7	+50 ± 7	−10 ± 7	1972–2000	−0.4 ± 0.2
ASTER DEM (2003) minus USGS (1972/73) DEM							
(7) Bering and Tana Glaciers	1015	−114 ± 4	−235 ± 5	+120 ± 5	−112 ± 5	1972–2003	−3.6 ± 0.2
SRTM (adjusted to 1999) minus USGS DEM (1972/73)							
(8) Bering Lobe	488	−43 ± 2	−160 ± 4		−88 ± 4	1972–99	−3.3 ± 0.1
(9) Central Moraine	282	−14 ± 1	−150 ± 4	+60 ± 4	−50 ± 4	1972–99	−1.8 ± 0.1
(10) Steller Lobe	192	−11 ± 1	−100 ± 5		−57 ± 5	1972–99	−2.0 ± 0.2
Bering Glacier system, 1972–2003							
(1) to (10)	3563		−191 ± 17		−54 ± 5		−1.7 ± 0.2

Notes: $A \equiv$ area; $\Delta V \equiv$ volume change; $\Delta E \equiv$ surface elevation change; $\Delta V/A \equiv$ area-average surface elevation change; $\Delta t \equiv$ time interval; $\Delta V/\overline{A}/t \equiv$ area-average surface elevation change rate.
The estimated uncertainty of the total mean volume change is given as the sum of the preceding uncertainties of each part in the summation.

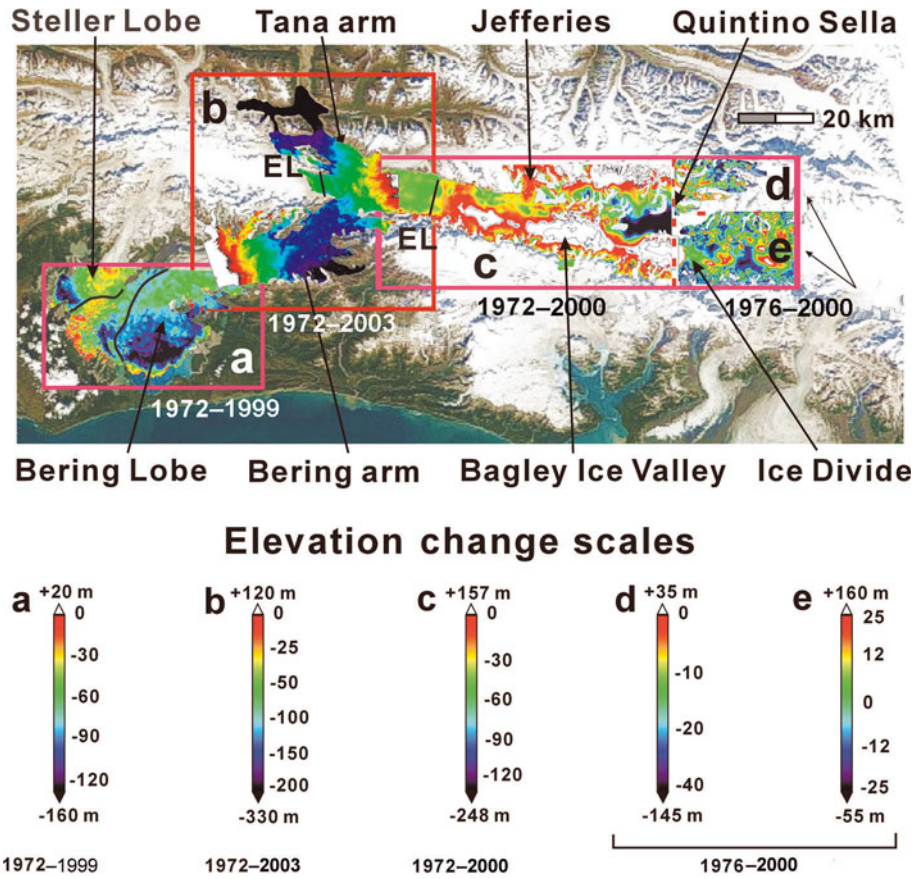

Fig. 5. Difference DEM surface-elevation changes on the Bering Glacier system from 1972 to 2003. Glacier mask areas are draped on the MODIS image of 9 September 2003. Red bounding boxes of the DEMs are shown. (a) SRTM (JPL) minus USGS DEM. (b) ASTER minus USGS DEM. (c) Intermap minus USGS DEM. (d) Intermap minus Canada DEM. (e) Intermap minus Canada DEM. Lines marked by EL denote the position of the long-term equilibrium lines. The bottom section gives the elevation-change scales and their time periods.

system below the long-term equilibrium lines (i.e. within ablation areas). Quintino Sella Glacier surface elevations were drawn down by the 1993–95 surge and by preceding surges, which occurred in 1965–66 and 1957–60. Surface elevations on Upper Seward Glacier and upper Quintino Sella (King Trench Glacier) show the smallest magnitudes of surface elevation changes (i.e. in high-elevation accumulation areas).

Integrating the volume changes on the parts of the Bering Glacier system shows a volume loss of $191 \pm 17.0\,\mathrm{km}^3$ from 1972 to 2003. Area-average surface elevation lowering was $54 \pm 5.0\,\mathrm{m}$ at a rate of $1.7 \pm 0.2\,\mathrm{m\,a}^{-1}$. The area covered is $3563\,\mathrm{km}^2$, about 70% of the estimated total area of the Bering Glacier system (Molnia, 2001). Our latest volume-loss estimate is much greater than our previous estimates, due to greater area coverage, and the Bering Glacier system experienced an acceleration of surface-area lowering following the 1993–95 surge (Arendt and others, 2002, 2006; Muskett and others, 2003).

Figure 6a shows glacier center-line elevation change profiles derived through differencing aircraft laser altimetry with the USGS DEM. The time periods of the profiles are from late summer 1972 to June 1995 (blue), to August 2000 (red) and to August 2003 (orange). The section of the profile from the beginning up to the 100 km mark is Bering Glacier. Bagley Ice Valley begins at the 100 km mark to the profile end, which is below the mouth of Quintino Sella Glacier. Elevation changes are non-uniform and largest on the Bering Glacier section (ablation area) of the profiles. An elevation–area distribution was used to estimate the volume and area–average elevation changes. From 1972 to June 1995 the volume loss was $41 \pm 4.3\,\mathrm{km}^3$ at a rate of $0.9 \pm 0.1\,\mathrm{m\,a}^{-1}$. During the 5 year interval 1995–2000 following the 1993–95 surge, volume loss was $30 \pm 4.3\,\mathrm{km}^3$ at a rate of $3.0 \pm 0.7\,\mathrm{m\,a}^{-1}$. During the 3 year interval 2000–03, volume loss was $7.1 \pm 1.3\,\mathrm{km}^3$ at a rate of $1.5 \pm 0.4\,\mathrm{m\,a}^{-1}$.

Figure 6b illustrates comparative surface elevations using a 1957 map compilation (by Post) with the elevations extracted from the 1972/73 USGS DEM and the 2000 Intermap DEM. Surface-elevation changes on Bagley Ice Valley and Quintino Sella Glacier at the dates of the map and DEMs indicate effects associated with the previous surges in 1993–95, 1965–66 and 1957–60.

NASA ICESat-derived surface-elevation changes

ICESat-to-ICESat and ICESat-Intermap DEM surface-elevation changes show non-uniform surface elevation rising and lowering (Fig. 7; Table 3). Surface-elevation changes across Bering Glacier and Bagley Ice Valley show large magnitudes from November 2004 to November 2006 and October 2003 to October 2006, respectively. Track 0416 crossings on Bagley Ice Valley at 1500 m elevation show a mean surface elevation lowering of $16 \pm 5.9\,\mathrm{m}$ (a range of 2.9 m on the sides to 28 m near the center) from 2003 to 2006. The green line connecting the red October 2006 footprint to the October 2003 footprint is 60 m long.

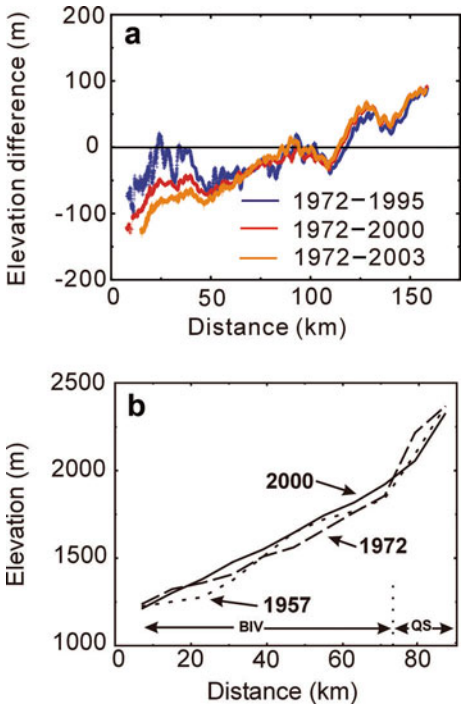

Fig. 6. Profiles of center-line surface-elevation changes on Bering Glacier, Bagley Ice Valley and Quintino Sella Glacier. (a) Center-line surface elevation differences on Bering Glacier and Bagley Ice Valley from aircraft laser altimetry. The transition from Bering Glacier to Bagley Ice Valley occurs near the 100 km nominal distance mark. (b) Center-line surface elevations along Bagley Ice Valley and Quintino Sella Glacier.

ASTER imagery from 2003 and 2006 confirms crevasses limited to the sides of Bagley Ice Valley. Track 0185 crossings on Bering Glacier show a mean surface elevation rising of 26.0 ± 19.7 m (a range of 3.9 m lowering on the sides to 53 m rising near the center) from 2004 to 2006. Notably, ICESat elevation changes of track 0185 from 2003 to 2004 show a mean surface elevation lowering of 0.8 ± 0.1 m; track 0416 (differenced on the Intermap DEM) shows surface elevation rising of 4.0 ± 0.4 m from September 2000 to September 2003.

Observation of outburst floods, May to September 2006

During May to September 2006, MODIS imagery (250 m resolution) indicated outburst flooding from the Bering terminus (Fig. 8). Imagery from late summers of 2003–04 shows Vitus Lake to be relatively free of turbid water discharges. Change in turbidity, relative to images from August and September 2004, was noticed on 30 May (Fig. 8a). Observations show the heaviest turbidity occurred on 12 July (Fig. 8b). August imagery shows a decrease in turbidity (Fig. 8c). By 25 September, turbidity had decreased to near the 2003–04 visual levels (Fig. 8d). Ground observations at Vitus Lake in August 2006 indicated subglacial discharge at points along the northeastern terminus (Liversedge, 2007). Satellite observations and ground reports in the summer of 2006 did not indicate a surge.

DISCUSSION

The surface-elevation lowering and volume losses of Bering Glacier and Bagley Ice Valley dominate the area-average surface elevation change, i.e. mass balance (Table 2; Fig. 5). Bagley Ice Valley, above the long-term equilibrium line at approximately 1100 m elevation to the mouth of Quintino Sella Glacier tributary, has experienced volume increases from 1972 to 2000. Columbus Glacier, the extension of Bagley Ice Valley above the mouth of Quintino Sella Glacier to the ice divide with Upper Seward Glacier, also has had a volume increase. This is in contrast to the volume decreases of Quintino Sella Glacier and the ice divide with Upper Seward Glacier. NASA Terra/ASTER observations (Fig. 9a) show clean and apparent dirty-water pools/debris patches from 9 August 2004 at high elevations on the center-line surface of Quintino Sella Glacier. Imagery prior to 2004 shows no rock avalanches onto the center line of Quintino Sella Glacier. This indicates impulse/rapid short-term sliding events. The rapid impulses overpressured and dilated the basal hydrologic system to in excess of overburden pressures, which ruptured the glacier from the base to the surface, where discharges of basal debris and water are consistent with surge dynamics (Raymond, 1987; Kavanaugh and Clarke, 2000; Roberts, 2005).

Table 3. ICESat-derived surface elevation changes

Glacier	Laser campaign	Track	Δt	$\overline{\Delta E}$	σ	$\sigma/\sqrt{N}$
				m	m	m
ICESat repeat tracks						
Bering	Laser 2A, 3A	0185	2003–04	–0.8	2.2	0.3
Bering	Laser 3A, 3G	0185	2004–06	+26.0	19.7	2.2
Waxell	Laser 2A, 3G	0185	2003–06	+1.4	1.8	0.3
Bagley	Laser 2A, 3G	0416	2003–06	–16.0	5.9	0.8
ICESat relative to the Intermap DEM						
Bagley	Laser 2A	1279	2000–03	+2.5	3.1	0.4
Bagley	Laser 2A	0416	2000–03	+4.0	3.1	0.4
Bagley	Laser 2A	1286	2000–03	+4.2	1.9	0.4
Bagley	Laser 3A	0423	2000–04	–1.6	0.9	0.2
Quintino Sella	Laser 3A	0423	2000–04	–1.6	0.9	0.2
Bagley	Laser 3A	0044	2000–04	+1.1	1.3	0.4
Quintino Sella	Laser 3A	0044	2000–04	–2.5	1.1	0.3

Notes: $\Delta t \equiv$ time interval; $\overline{\Delta E} \equiv$ mean elevation change; $\sigma \equiv$ standard deviation of the mean; $\sigma/\sqrt{N} \equiv$ uncertainty of the mean; $N \equiv$ number of ICESat points.

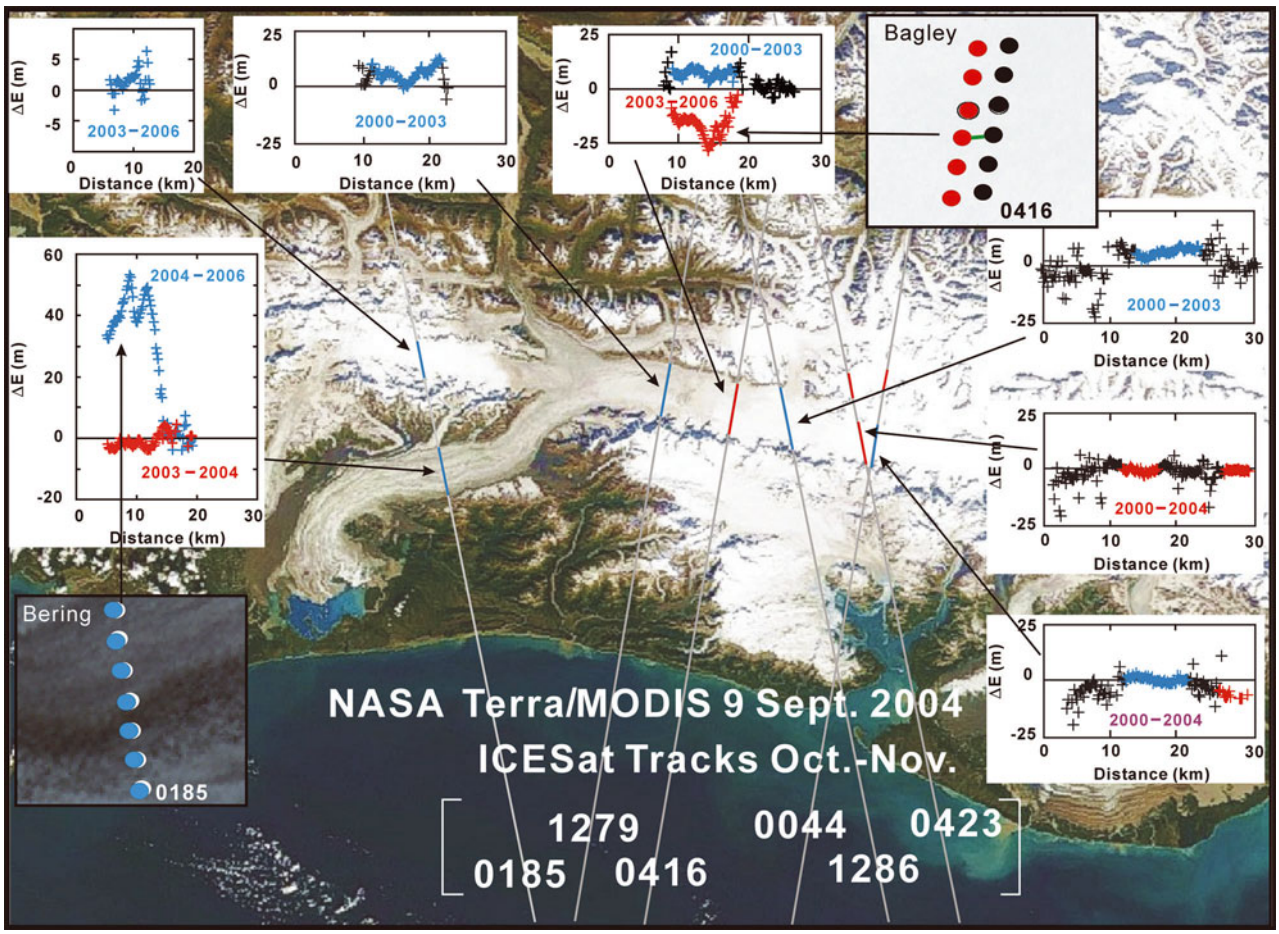

Fig. 7. ICESat-derived surface-elevation differences on the Bering Glacier system from 2000 to 2006. Noteworthy repeat-pass footprints on Bering, track 0185, and Bagley, track 0416 (green line is 60 m long), are shown (ASTER images August 2003 and 2006 in the panels, respectively). Filled circle diameters are 70 m. Surface-elevation differences from 2000 to 2003/04 are relative to the Intermap DEM. Surface-elevation changes on the colored (red and blue) line segments are given in Table 2. Datum is WGS84.

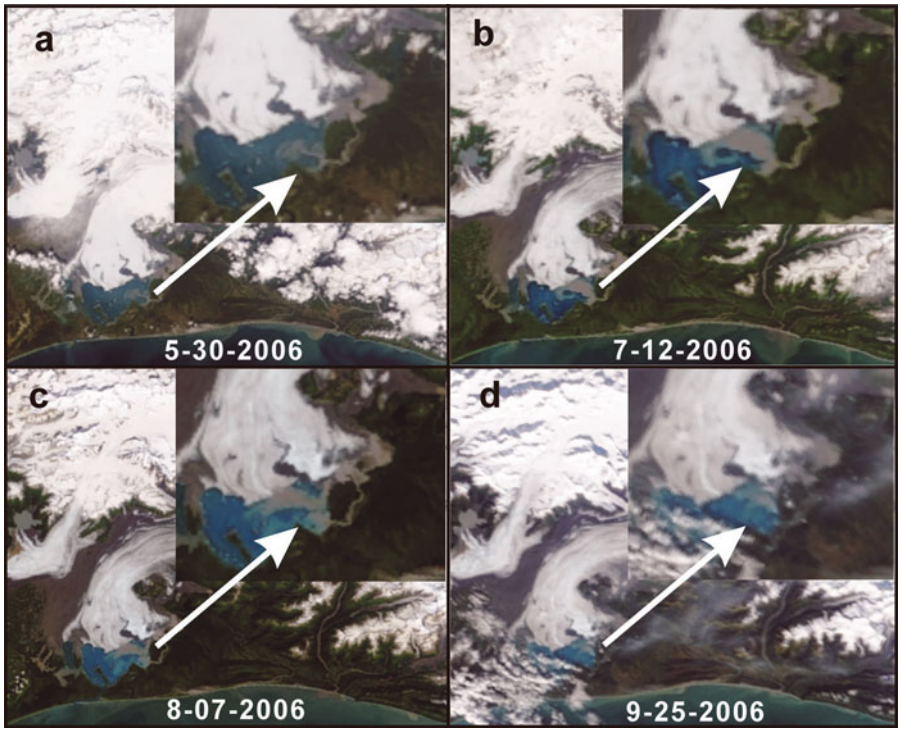

Fig. 8. NASA Terra/MODIS images of Bering Glacier and Vitus Lake showing basal-water discharge outburst floods during May to September 2006: (a) 30 May, (b) 12 July, (c) 7 August, (d) 25 September. Comparison of the NASA Terra/MODIS images shows the state of Vitus Lake on 9 September 2004 compared with the outburst flood discharging muddy water on 7 August 2006.

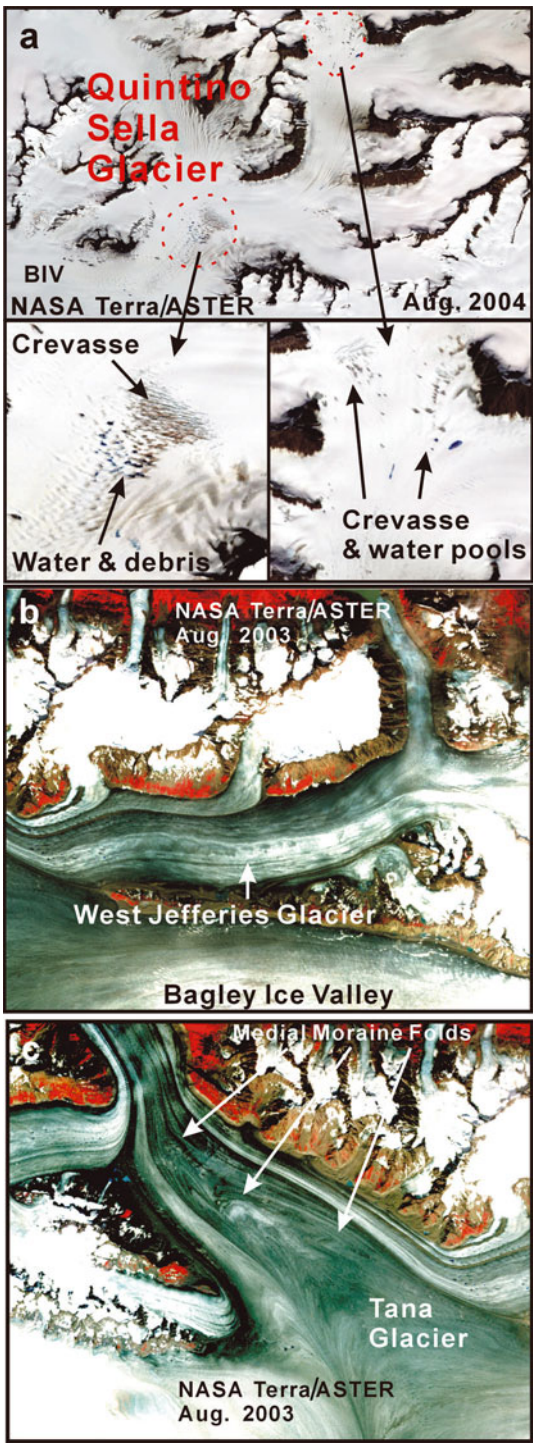

Fig. 9. NASA Terra/ASTER images of Quintino Sella, Jefferies and Tana Glaciers. (a) ASTER image from August 2004 showing center flowband crevasse, water and apparent debris indicating an impulse event. (b) ASTER image showing wavy medial moraines on Jefferies Glacier, August 2003. (c) ASTER image of Tana Glacier, August 2003, showing medial moraine folds indicating non-steady flow.

The regions of increased volume on Bagley Ice Valley, with their spatially non-uniform surface-elevation changes, spread in longitudinal extent down-glacier. We interpret this as an indication of flow diffusion as ice masses from the source regions, Quintino Sella Glacier and the ice divide, are moved down-glacier by surge dynamics.

The arm of East Jefferies Glacier had non-uniform elevation changes and volume loss from 1972 to 2000. Medial moraines of West Jefferies Glacier observed on 8 August 2003 (NASA Terra/ASTER; Fig. 9b) have a wavy character, but to our knowledge the glacier has not been observed surging.

To our knowledge, Tana Glacier has not been observed surging. Observations of folded medial moraines from 8 August 2003 (NASA Terra/ASTER) indicate a non-steady flow/sliding character (Fig. 9c).

Sediment-laden basal-water discharges from glacier termini are a key indicator of the end-event of surges, and mini-surges (Raymond, 1987; Kavanaugh and Clarke, 2000; Roberts, 2005). Overpressurization of the englacial water storage system through impulse/rapid short-term sliding events, also known to enable surging, can lead to clean and muddy water discharges on the glacier surface, which have no connection to surface-water streamflows. NASA Terra/MODIS images from late-spring to summer of 2006 show muddy water flood-discharging from the northeastern terminus of the Bering Lobe and into Vitus Lake. By 12 July, almost a third of Vitus Lake became turbid from the basal discharge. By 7 August, the turbidity of the right third of Vitus Lake had reduced, with discharge ongoing. On 7 August (Fig. 8d), basal discharge appeared much reduced and the waters of Vitus Lake returned to their pre-flood condition. Muddy water discharge into Tsivieta Lake was also observed on the ground (Liversedge, 2007). Similar surface-elevation changes and basal-water transfer have been reported from the Antarctic subglacial lakes (Fricker and others, 2007). Our observations of the basal–englacial water transfer events support the interpretation of interferometric SAR (InSAR) phase bull's-eye generation and association with the evolution of the basal hydrologic system of the Bering Glacier system as observed by Fatland (1998) and Fatland and Lingle (2002). If we assume basal-water transfer and surface-elevation changes began in March 2006 and ended by July 2006, a period of 122 days, the mean rate of surface-elevation lowering on Bagley Ice Valley would have been $0.13 \pm 0.05\,\mathrm{m\,d^{-1}}$, and the mean rate of surface-elevation rise on Bering Glacier would have been $0.21 \pm 0.16\,\mathrm{m\,d^{-1}}$.

CONCLUSIONS

In the coastal mountains of south-central Alaska and Yukon, the Bering Glacier system is the largest and possibly most complex association of surge and non-surge temperate glaciers in North America. NASA Terra/MODIS observations in the spring and summer of 2006 indicated outburst floods of muddy water from the Bering terminus. ICESat-derived observations of surface-elevation changes from October 2003 to October 2006 and November 2004 to November 2006 indicate surface-elevation lowering on Bagley Ice Valley (down as much as 28 m) and surface-elevation rise on Bering Glacier (up as much as 53 m). These observations indicate basal–englacial hydrologic system dynamics affecting the surface elevations in the absence of surge dynamics.

We estimate the Bering Glacier system volume loss was $191 \pm 17\,\mathrm{km^3}$, at a rate of $1.7 \pm 0.2\,\mathrm{m\,a^{-1}}$, during 1972–2003. This estimate covers $3563\,\mathrm{km^2}$, about 70% of the total area of the glacier system. The main flowband of the glacier system, Bering Glacier and Bagley Ice Valley, experienced surface-elevation lowering of $0.9 \pm 0.1\,\mathrm{m\,a^{-1}}$ during 1972–95. This accelerated to $3.0 \pm 0.7\,\mathrm{m\,a^{-1}}$ during 1995–2000, following the 1993–95 surge. Then during 2000–03, surface-elevation lowering was $1.5 \pm 0.4\,\mathrm{m\,a^{-1}}$.

ACKNOWLEDGEMENTS

We thank the NASA Cryosphere Sciences Program for supporting grants NAG5-11336, NAG5-12914, NAG5-13760 and NAG5-9901; the Interdisciplinary Science in the NASA Earth Science Enterprise for support with grant NNG04GH64G; the NASA Scientific Data Purchase Program for funding the acquisition and processing of the Bagley Ice Valley DEM by Intermap Technologies, Inc. (project No. 00241-311); H. Gansen, T. Kuuskivi and the engineers and technicians of Intermap for their excellent work; the DLR's S. Dech and A. Roth for supporting outside-schedule processing of the SRTM X-band data over southern Alaska, and W. Knoepfle for providing assistance during mosaicking of the SRTM X-band DEM; and the NASA Scientific Data Purchase Program for funding acquisition and processing by Intermap Technologies, Inc. of the Bagley Ice Valley and Malaspina Glacier system DEMs. We thank the US National Geospatial-Intelligence Agency (NGA, formerly the National Imagery and Mapping Agency (NIMA)) for supporting this work with University Research Initiative (NURI) grant NMA501-03-1-2026; and the US National Science Foundation Office of Polar Programs Arctic Natural Sciences for supporting this work through grant ARC-0612537. We thank NASA's Ice, Cloud and land Elevation Satellite project and the US National Snow and Ice Data Center for providing ICESat data and visualization computer programs. We thank C. Larson for discussions and for making available the aerial photography of Bering Glacier he acquired during the spring 2007 field season, and K. Engle for assistance with SAR processing of ERS-1/-2 tandem mission datasets in an early phase of this research and acquiring NASA Terra/MODIS imagery. We thank T. Logan, now with the Alaska Region Supercomputing Center, who as a technician at the Alaska Satellite Facility (ASF) played the lead role in developing the first generation of synthetic aperture radar processing tools (at ASF) for UNIX-based computer systems. We thank R. Guritz of ASF. The Japan Aerospace Exploration Agency is thanked for computer facility support at the International Arctic Research Center. The Geographic Information Network of Alaska (K. Engle) provided the NASA Terra/MODIS imagery. We thank A. Arendt and P. Clause (pilot) for the small-aircraft altimetry acquired in August 2003. Support for J. Sauber was provided by the NASA Earth Surface and Interior program. R. Muskett thanks the International Arctic Research Center for facility support. An anonymous reviewer is thanked for constructive comments.

REFERENCES

Abrams, M. and S. Hook. 2002. *ASTER user's handbook, Version 2*. Pasadena, CA, NASA Jet Propulsion Laboratory.

Alford, D. 1967. Density variations in alpine snow. *J. Glaciol.,* **6**(46), 495–503.

Anonymous. 1969. Mass-balance terms. *J. Glaciol.,* **8**(52), 3–7.

Arendt, A.A., K.A. Echelmeyer, W.D. Harrison, C.S. Lingle and V.B. Valentine. 2002. Rapid wastage of Alaska glaciers and their contribution to rising sea level. *Science,* **297**(5580), 382–386.

Arendt, A. *and 7 others*. 2006. Updated estimates of glacier volume changes in the western Chugach Mountains, Alaska, and a comparison of regional extrapolation methods. *J. Geophys. Res.,* **111**(F3), F03019. (10.1029/2005JF000436.)

Bader, H. 1954. Sorge's Law of densification of snow on high polar glaciers. *J. Glaciol.,* **2**(15), 319–323.

Bartholomaus, T.C., R.S. Anderson and S.P. Anderson. 2008. Response of glacier basal motion to transient water storage. *Nature Geosci.,* **1**(1), 33–37.

Beedle, M.J. *and 7 others*. 2008. Improving estimation of glacier volume change: a GLIMS case study of Bering Glacier System, Alaska. *Cryosphere,* **2**(1), 33–51.

Echelmeyer, K.A. *and 8 others*. 1996. Airborne surface profiling of glaciers: a case-study in Alaska. *J. Glaciol.,* **42**(142), 538–547.

Eineder, M., H. Breit, N. Adam, J. Holzner, S. Suchandt and B. Rabus. 2001. SRTM X-SAR calibration results. In *Proceedings of International Geoscience and Remote Sensing Symposium (IGARSS 2001), 9–13 July 2001, Sydney, Australia. Vol. 2*. Piscataway, NJ, Institute of Electrical and Electronics Engineers, 748–750.

Farr, T.G. *and 17 others*. 2007. The Shuttle Radar Topography Mission. *Rev. Geophys.,* **45**(2), RG2004. (10.1029/2005RG000183.)

Fatland, D.R. 1998. Studies of Bagley Icefield during surge and Black Rapids Glacier, Alaska, using spaceborne SAR interferometry. (PhD thesis, University of Alaska Fairbanks.)

Fatland, D.R. and C.S. Lingle. 2002. InSAR observations of the 1993–95 Bering Glacier (Alaska, U.S.A.) surge and a surge hypothesis. *J. Glaciol.,* **48**(162), 439–451.

Fountain, A.G. and J.S. Walder. 1998. Water flow through temperate glaciers. *Rev. Geophys.,* **36**(3), 299–328.

Fricker, H.A., T. Scambos, R. Bindschadler and L. Padman. 2007. An active subglacial water system in West Antarctica mapped from space. *Science,* **315**(5818), 1544–1548.

Geudtner, D., M. Zink, C. Gierull and S. Shaffer. 2002. Interferometric alignment of the X-SAR antenna system on the space shuttle radar topography mission. *IEEE Trans. Geosci. Remote Sens.,* **40**(5), 995–1006.

Harrison, W.D. and A.S. Post. 2003. How much do we really know about glacier surging? *Ann. Glaciol.,* **36**, 1–6.

Helm, A., A. Braun, S. Eickschen and T. Schöne. 2002. Calibration of the shuttle radar topography mission X-SAR instrument using a synthetic altimetry data model. *Can. J. Remote Sens.,* **28**(4), 573–580.

Intermap Technologies Corporation. 2006. *Global terrain product handbook.* Ottawa, Ont., Intermap Technologies Corp.

Kavanaugh, J.L. and G.K.C. Clarke. 2000. Evidence for extreme pressure pulses in the subglacial water system. *J. Glaciol.,* **46**(153), 206–212.

Kieffer, H.H., K.F. Mullins and D.J. MacKinnon. 2008. Validation of the ASTER instrument level 1A scene geometry. *Photogramm. Eng. Remote Sens.,* **74**(3), 289–302.

Li, S. 1999. Summer environmental mapping potential of a large-scale ERS-1 SAR mosaic of the state of Alaska. *Int. J. Remote Sensing,* **20**(2), 387–401.

Lingle, C.S. and D.R. Fatland. 2003. Does englacial water storage drive temperate glacier surges? *Ann. Glaciol.,* **36**, 14–20.

Liversedge, L.K. 2007. Turbidity mapping and prediction in ice marginal lakes at the Bering Glacier system, Alaska. (MS thesis, University of Michigan.)

Matthews, J.P., X.-D. Yang, J. Shen and T. Awaji. 2008. Structured Sun glitter recorded in an ASTER along-track stereo image of Nam Co Lake (Tibet): an interpretation based on supercritical flow over a lake floor depression. *J. Geophys. Res.,* **113**(C1), C01019. (10.1029/2007JC004204.)

Meier, M.F. 1962. Proposed definitions for glacier mass budget terms. *J. Glaciol.,* **4**(33), 252–263.

Molnia, B. F. 2001. Glaciers of Alaska. *Alaska Geogr.,* **28**(2).

Molnia, B.F. and A. Post. 1995. Holocene history of Bering Glacier, Alaska: a prelude to the 1993–1994 surge. *Phys. Geogr.,* **16**(2), 87–117.

Moore, G.W.K., G. Holdsworth and K. Alverson. 2002. Climate change in the North Pacific region over the past three centuries. *Nature,* **420**(6914), 401–403.

Muskett, R. 2007. Mass balances and dynamic changes of the Bering, Malaspina, and Icy Bay glacier systems of Alaska, U.S.A., and Yukon, Canada. (PhD thesis, University of Alaska Fairbanks.)

Muskett, R.R., C.S. Lingle, W.V. Tangborn and B.T. Rabus. 2003. Multi-decadal elevation changes on Bagley Ice Valley and Malaspina Glacier, Alaska. *Geophys. Res. Lett.,* **30**(16), 1857. (10.1029/2003GL017707.)

Muskett, R.R., C.S. Lingle, J.M. Sauber, B.T. Rabus and W.V. Tangborn. 2008a. Acceleration of surface lowering on the tidewater glaciers of Icy Bay, Alaska, U.S.A. from InSAR DEMs and ICESat altimetry. *Earth Planet. Sci. Lett.,* **265**(3–4), 345–359.

Muskett, R.R., C.S. Lingle, J.M. Sauber, A.S. Post, W.V. Tangborn and B.T. Rabus. 2008b. Surging, accelerating surface lowering and volume reduction of the Malaspina Glacier system, Alaska, USA, and Yukon, Canada, from 1972 to 2006. *J. Glaciol.,* **54**(188), 788–800.

National Imagery and Mapping Agency (NIMA). 2000. *Department of Defense World Geodetic System 1984: its definition and relationships with local geodetic systems. Third edition.* Washington, DC, Department of Defense. (NIMA Tech. Rep. 8350.2.)

Natural Resources Canada. 1996. *Standards and specifications of the National Topographic Data Base, Version 3.1*. Ottawa, Ont., Natural Resources Canada. Centre for Topographical Information.

Partington, K.C. 1998. Discrimination of glacier facies using multi-temporal SAR data. *J. Glaciol.,* **44**(146), 42–53.

Post, A. 1972. Periodic surge origin of folded medial moraines on Bering piedmont glacier, Alaska. *J. Glaciol.,* **11**(62), 219–226.

Rabus, B., M. Eineder, A. Roth and R. Bamler. 2003. The shuttle radar topography mission – a new class of digital elevation models acquired by spaceborne radar. *ISPRS J. Photogramm. Eng. Remote Sens.,* **57**(4), 241–262.

Rapp, R.H. 1998. The EGM96 geoid undulation with respect to the SGS84 ellipsoid. *NASA Tech. Pap.* 1998-206861, ch.11, 1–6.

Raymond, C.F. 1987. How do glaciers surge? A review. *J. Geophys. Res.,* **92**(B9), 9121–9134.

Rignot, E.J.M. and J.J. van Zyl. 1993. Change detection techniques for ERS-1 SAR data. *IEEE Trans. Geosci. Remote Sens.,* **31**(4), 896–906.

Rignot, E., K. Echelmeyer and W. Krabill. 2001. Penetration depth of interferometric synthetic-aperture radar signals in snow and ice. *Geophys. Res. Lett.,* **28**(18), 3501–3504.

Roberts, M.J. 2005. Jökulhlaups: a reassessment of floodwater flow through glaciers. *Rev. Geophys.,* **43**(1), RG1002. (10.1029/2003RG000147.)

Roth, A., A. Eineder, B. Rabus, E. Mikusch and B. Schattler. 2001. SRTM/X-SAR: products and processing facility. In *Proceedings of the International Geoscience and Remote Sensing Symposium (IGARSS 2001), 9–13 July 2001, Sydney, Australia. Vol. 2*. Piscataway, NJ, Institute of Electrical and Electronic Engineers, 745–747.

Roush, J.J., C.S. Lingle, R.M. Guritz, D.R. Fatland and V.A. Voronina. 2003. Surge-front propagation and velocities during the early-1993–95 surge of Bering Glacier, Alaska, U.S.A., from sequential SAR imagery. *Ann. Glaciol.,* **36**, 37–44.

Scambos, T.A., J.A. Bohlander, C.A. Shuman and P. Skvarca. 2004. Glacier acceleration and thinning after ice shelf collapse in the Larsen B embayment, Antarctica. *Geophys. Res. Lett.,* **31**(18), L18402. (10.1029/2004GL020670.)

Schutz, B.E., H.J. Zwally, C.A. Shuman, D. Hancock and J.P. DiMarzio. 2005. Overview of the ICESat Mission. *Geophys. Res. Lett.,* **32**(21), L21S01. (10.1029/2005GL024009.)

Sharp, R.P. 1951. Accumulation and ablation on the Seward–Malaspina Glacier system, Canada–Alaska. *Geol. Soc. Am. Bull.,* **62**(7), 725–743.

Sharp, R.P. 1958. Malaspina Glacier, Alaska. *Geol. Soc. Am. Bull.,* **69**(2), 617–646.

Smith, D.A. and D.R. Roman. 2001. GEOID99 and G99SSS: 1-arc-minute geoid models for the United States. *J. Geod.,* **75**(9–10), 469–490.

Tangborn, W. 1999. A mass balance model that uses low-altitude meteorological observations and the area–altitude distribution of a glacier. *Geogr. Ann.,* **81A**(4), 753–765.

Toller, G.N. and A. Isaacman. 2003. *MODIS Level 1B product user's guide.* Greenbelt, MD, NASA Goddard Space Flight Center.

Toutin, T. 2008. ASTER DEMs for geomatic and geoscientific applications: a review. *Int. J. Remote Sensing,* **29**(7), 1855–1875.

US Geological Survey (USGS). 1990. *Digital elevation models: data users' guide 5.* Reston, VA, US Department of the Interior. US Geological Survey.

Yamaguchi, Y., A.B. Kahle, H. Tsu, T. Kawakami and M. Pniel. 1998. Overview of Advanced Spaceborne Thermal Emission and Reflection Radiometer (ASTER). *IEEE Trans. Geosci. Remote Sens.,* **36**(4), 1062–1071.

Zhang, J., U.S. Bhatt, W.V. Tangborn and C.S. Lingle. 2007. Climate downscaling for estimating glacier mass balances in northwestern North America: validation with a USGS benchmark glacier. *Geophys. Res. Lett.,* **34**(21), L21505. (10.1029/2007GL031139).

Zwally, H.J. and J. Li. 2002. Seasonal and interannual variations of firn densification and ice-sheet surface elevation at Greenland summit. *J. Glaciol.,* **48**(161), 199–207.

MS received 25 January 2008 and accepted in revised form 23 October 2008